A Multiscale Wavelet Data Treatment for Reliable Localization of Inflection Points for Analytical Purposes

Valdomiro Lacerda Martins,[†,‡] Luciano Farias de Almeida,[†,‡] Suzana Limeira de Castro,[‡] Roberto Kawakami Harrop Galvão,[§] Mário César Ugulino de Araújo,*[,‡] and Edvan Cirino da Silva[‡]

Departamento de Química Fundamental, Universidade Federal de Pernambuco, CCEN, CEP 50740-901 - Recife PE, Brazil, Departamento de Química, Universidade Federal da Paraíba, CCEN, Caixa Postal 5093, CEP 58051-970 - João Pessoa, PB, Brazil, and Divisão de Engenharia Eletrônica, Instituto Tecnológico de Aeronáutica, CEP 12228-900 - São José dos Campos, SP, Brazil

Received June 8, 2003

Instrumental analysis techniques that employ measurements based on inflection points may have their accuracy compromised due to the need for signal differentiation, which is very sensitive to instrumental noise. This paper presents a strategy for localizing inflection points that exploits the multiscale processing capability of the Wavelet Transform and avoids the need for explicit signal differentiation. The strategy is illustrated in simulated examples and also in a real analytical problem involving the determination of Pb and Cd by potentiometric stripping analysis. In this application, the results were in good agreement with the expected values and were slightly better than those obtained from the first derivative of the curves after smoothing by a Windowed Fourier Transform.

INTRODUCTION

The Wavelet Transform (WT) has been acknowledged as an efficient tool for the treatment of instrumental signals. Its use in multivariate calibration problems, for instance, has been well-established in several recent works in the analytical chemistry literature.[1−9] The WT has also been successfully employed for the localization of characteristic points in signals, due to its distinctive features of localized processing and multiscale analysis.[10−14] Moreover, in denoising applications, it has been reported[15,16] that the WT is less likely to distort peaks, valleys, and inflection points than other smoothing techniques such as boxcar filtering, moving average, Fourier transform, and running polynomial smoothers (Savitzky-Golay method).[17]

Among the applications of WT for multiscale localization and characterization of signal features, one could cite the work of Liu et al.,[12] which was aimed at detecting the onset time of localized corrosion in Al 7075-T76 (UNS A97075) in 3.5% sodium chloride solution containing different inhibiting pigments on the basis of the analysis of electrochemical potential noises; the work of Sadler et al.,[18,19] which concerned the quantification of the absorbance profile obtained during graphite-furnace atomic absorption spectrometry; and the work of Bos and Hoogendam,[20] which applied WT to the determination of peak intensities in flow-injection analysis in order to minimize the effects of noise and baseline drift. Many applications have also been reported in other fields, such as mechanical[13] and biomedical[14] engineering.

Instrumental analysis techniques that employ measurements based on inflection points (potentiometric stripping analysis, potentiometric titration, and thermogravimetry, for example)[21] may have their accuracy compromised because of the need to differentiate the signal. In fact, differentiation is very sensitive to instrumental noise and may not provide a clear indication of the localization of the inflection points.

In this context, this paper presents a strategy for localizing inflection points that exploits the multiscale processing capability of WT and avoids the need for explicit signal differentiation. The theoretical aspects involved are discussed, and simulated examples are presented to illustrate the proposed strategy. A real analytical problem involving the determination of Pb and Cd at low concentration levels by potentiometric stripping analysis (PSA) is also investigated.[22,23] To illustrate the utility of the proposed strategy to deal with analytical measurements with low signal-to-noise ratio, a lab-made potentiostat/galvanostat was employed in the experiment.

THEORETICAL BASIS

Notation. $\mathcal{R}$ and $\mathcal{R}^*$ denote the set of real numbers with and without zero, respectively. $L^2(\mathcal{R})$ denotes the Hilbert space of functions f: $\mathcal{R} \rightarrow \mathcal{R}$ such that

$$\int_{-\infty}^{+\infty} |f(t)|^2 dt < \infty \tag{1}$$

The norm of the $L^2(\mathcal{R})$ space is defined as

$$||f|| = \left(\int_{-\infty}^{+\infty} |f(t)|^2 dt\right)^{1/2} \tag{2}$$

Given two functions $f, g \in L^2(\mathcal{R})$, their inner product is defined as

$$\langle f,g \rangle = \int_{-\infty}^{+\infty} f(t)g(t)dt \tag{3}$$

* Corresponding author phone: +55 83 216-7438; fax: +55 83 216-7437; e-mail: laqa@quimica.ufpb.br.
† Universidade Federal de Pernambuco.
‡ Universidade Federal da Paraíba.
§ Instituto Tecnológico de Aeronáutica.

10.1021/ci034112w CCC: $25.00
Published on Web 09/13/2003

and their convolution as

$$(f * g)(t) = \int_{-\infty}^{+\infty} f(\tau)g(t-\tau)d\tau \tag{4}$$

The support I_f of a function f: $\mathcal{R} \rightarrow \mathcal{R}$ is the largest set such that $f(t) \neq 0$, $\forall t \in I_f$. If I_f is an interval with limits t_1, t_2, then the support width of f is defined as $D_f = t_2 - t_1$.

Wf indicates the wavelet transform of signal f.

The Wavelet Transform. WT is an analysis tool that provides a picture about how the frequency content of a signal $f(t)$ evolves with time.[24−27] WT is obtained as the inner product of $f(t)$ with a family of wavelet functions $\psi_{a,b}$ defined from a single mother function $\psi \in L^2(\mathcal{R})$ as

$$\psi_{a,b}(t) = \frac{1}{|a|^{1/2}}\psi\left(\frac{t-b}{a}\right) \tag{5}$$

where $a \in \mathcal{R}^*$ and $b \in \mathcal{R}$ are termed scale and translation parameters, respectively. The factor $1/|a|^{1/2}$ is used for normalization and ensures that all wavelets have unit norm in $L^2(\mathcal{R})$. WT is thus a mapping from $\mathcal{R}^* \times \mathcal{R}$ to $\mathcal{R}$ defined[24−27] as

$$Wf(a,b) = < f,\psi_{a,b} > = \int_{-\infty}^{+\infty} f(t)\psi_{a,b}(t)dt \tag{6}$$

The inversibility of this transformation requires that the mean of ψ is zero.[24] Apart from this condition, ψ is usually chosen to have good localization in both time and frequency domains, in the sense that $\psi(t)$ and its Fourier transform $\Psi(\omega)$ rapidly decay to zero when $|t| \rightarrow \infty$ and $|\omega| \rightarrow \infty$, respectively. In this manner, the wavelet transform $Wf(a,b)$ can capture components of the signal in well-localized time-frequency windows.

It is interesting to point out that WT can be written as a convolution integral.[10] In fact, denoting by $\bar{\psi}$ the time-reversed version of ψ, that is

$$\bar{\psi}(t) = \psi(-t) \tag{7}$$

and by $\bar{\psi}_a$ the dilated version of $\bar{\psi}$, that is

$$\bar{\psi}_a(t) = \frac{1}{|a|^{1/2}}\bar{\psi}\left(\frac{t}{a}\right) \tag{8}$$

then it follows from eqs 5−8 that

$$Wf(a,b) = \int_{-\infty}^{+\infty} f(t)\bar{\psi}_a(b-t)d\tau = (f * \bar{\psi}_a)(b) \tag{9}$$

Notice that, if the wavelet is an even function (a symmetrical function around $t = 0$), that is, $\psi(t) = \psi(-t) = \bar{\psi}(t)$, then ψ itself can be used in the convolution integral, that is

$$Wf(a,b) = (f * \psi_a)(b) \tag{10}$$

Localization of Inflection Points. Given a function $f(t)$, the localization of an inflection point for which $d^2f/dt^2 = 0$ can be accomplished by using wavelet functions $\psi(t)$ obtained from smoothing functions. Smoothing functions are real-valued functions $\theta(t)$ that are localized in time (that is, decay to zero rapidly when $|t| \rightarrow \infty$) and whose integral is different from zero.[10] A typical example is the Gaussian function $\theta(t) = \exp(-t^2/2)$. The use of a smoothing function in a convolution integral has the effect of a moving-average filtering process.[17]

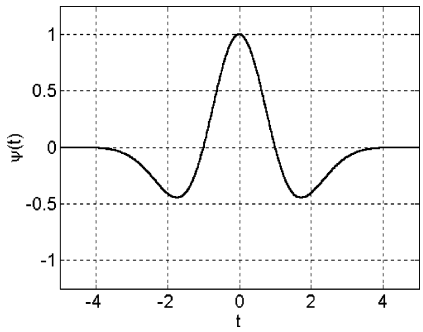

Figure 1. Mexican Hat wavelet.

Let $\psi(t)$ be proportional to the second derivative of a smoothing function $\theta(t)$, that is

$$\psi = k\frac{d^2\theta}{dt^2} \tag{11}$$

where k is a constant factor. For simplicity, assume that $\psi(t)$ is an even function, so that eq 10 is valid. This is the case, for instance, of the Mexican Hat wavelet $\psi(t) = (1-t^2)\exp(-t^2/2)$, shown in Figure 1, which is the second derivative of the Gaussian function with a change of sign ($k = -1$ in eq 11).

Denoting by θ_a the dilated version of θ, that is

$$\theta_a(t) = \frac{1}{|a|^{1/2}}\theta\left(\frac{t}{a}\right) \tag{12}$$

then eq 10 can be rewritten as

$$Wf(a,b) = ka^2\left(f * \frac{d^2\theta_a}{dt^2}\right)(b) \tag{13}$$

Equation 13 can be rewritten on the basis of the following property of convolution integrals[28]

$$f * \frac{d^n g}{dt^n} = \frac{d^n f}{dt^n} * g \tag{14}$$

for any functions f, $g \in L^2(\mathcal{R})$ and any integer $n > 0$. Equations 13 and 14 yield

$$Wf(a,b) = ka^2\left(\frac{d^2 f}{dt^2} * \theta_a\right)(b) \tag{15}$$

that is, the transform at each scale a is proportional to the second derivative of f smoothed by θ_a. As a result, the inflection point can be localized by searching for a zero-crossing of $Wf(a,b)$ along the b-axis. It should be noticed that the smoothing process may cause a shifting of the inflection point. As it will be shown in a simulated example, this shifting occurs when $f(t)$ is not symmetrical around the inflection point. However, the shifting becomes less important as the scale becomes smaller, so that, in the limit $a \rightarrow 0$, the zero-crossing position will correspond exactly to the desired inflection point.

It should be noticed that, in the presence of noise, crossing points at small scales may not be reliable, and thus it is not possible to localize the inflection point by directly analyzing

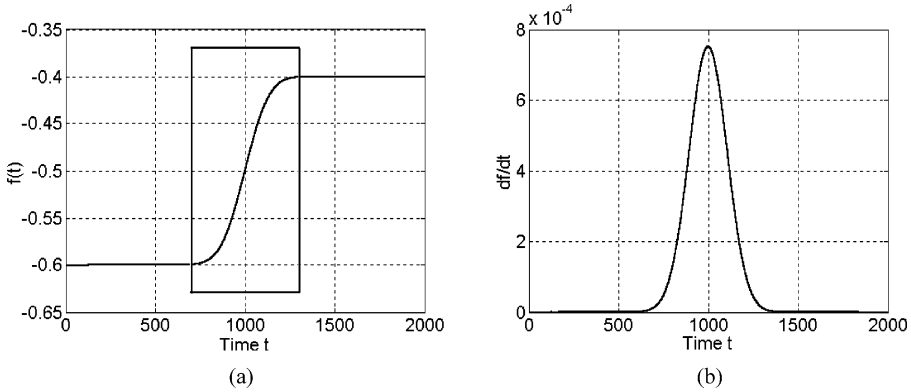

Figure 2. (a) Simulated sigmoidal signal with an inflection point at $t = 1000$. The gray box indicates the region selected for analysis. (b) First derivative of the signal.

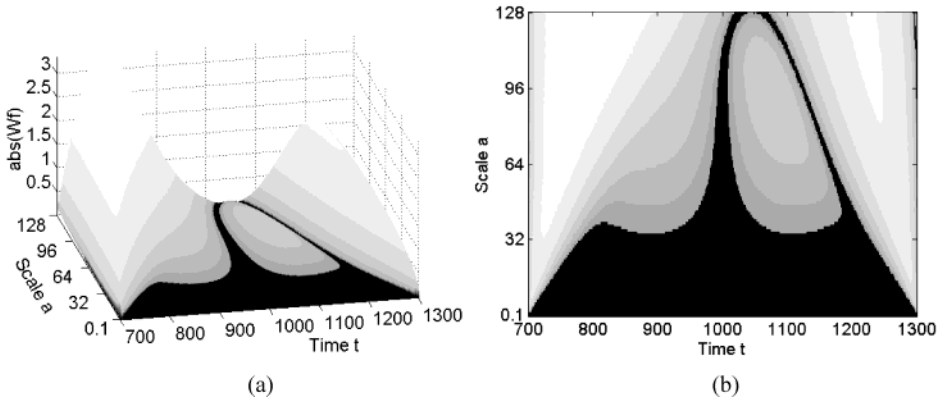

Figure 3. (a) Absolute value of the WT of the simulated sigmoidal signal. (b) Top view of the surface in (a).

the WT result for $a \rightarrow 0$. This problem is circumvented in this work by taking the zero-crossing of the WT at large scales and by using a linear extrapolation to estimate the position of the zero-crossing at $a = 0$. On the other hand, the use of too large scales is not recommended because of border effect problems.

In the convolution process, a border effect occurs when the translation parameter b is such that the wavelet support falls outside the interval where function f is defined. To complete the convolution operation, f is usually assumed to be zero outside this interval. Such procedure will generally cause a shift in the zero-crossing position of WT. Periodic or symmetric extensions of f may be employed to alleviate this problem, but in general it is not possible to eliminate it completely.

The border effect compromises the determination of the inflection point when the wavelet $\psi_{a,b}$ has a support that contains the inflection point and also one of the borders of f. It is worth noting that some mother wavelets do not have a finite support width. It is the case, for instance, of the Mexican Hat wavelet depicted in Figure 1. In this case, the support I_ψ should be replaced by an effective support, that is, an interval in which $|\psi(t)|$ is considerably larger than zero. For the Mexican Hat, an appropriate choice for this interval would be $[-2, +2]$, which results in an effective support width of 4.

Proposed Procedure for Choosing the Scales for the Analysis. To achieve a compromise between minimizing the effect of noise and avoiding border effects, a heuristic procedure to choose the scales that will be included in the extrapolation is proposed here.

First, the analyst should select a time window defining the region where the inflection point is to be searched. Let t_{min} and t_{max} be the boundaries of this window and $d = t_{max} - t_{min}$ be the window width. The value of d automatically defines the maximum scale to be employed. In fact, by adopting an effective support width of 4 for the Mexican Hat wavelet, the largest wavelet that fits inside the window is at scale $d/4$. However, this wavelet cannot be translated without falling outside the window. Thus, a reasonable choice is to take the largest scale as $a_{max} = d/8$. The smallest scale that can be reliably employed depends on the noise level. As a rule of thumb, a reasonable choice is to take the smallest scale as $a_{min} = a_{max}/2 = d/16$. To allow a more reliable fitting of the straight line that leads to the inflection point, three other scales, equally spaced between a_{min} and a_{max}, were employed in this work. Thus, the extrapolation procedure for determining the inflection point is based on WT at five scales: a_{max}, $7a_{max}/8$, $6a_{max}/8$, $5a_{max}/8$, and a_{min}.

SIMULATED EXAMPLES

Detection in the Absence of Noise. Figure 2a presents a simulated sigmoidal signal with an inflection point at $t = 1000$ (as can be seen from the peak of the first derivative in Figure 2b). The gray box indicates the region selected for analysis ($t = 700-1300$). In this case, $d = 600$, $a_{min} = 37.5$, and $a_{max} = 75$.

The Mexican Hat WT of this signal is depicted, in absolute value, in Figure 3a. Since the mother wavelet $\psi(t)$ is symmetric about $t = 0$ (Figure 1), the wavelet transform $Wf(a,b)$ for a given value of the translation parameter b captures features of the signal $f(t)$ around time $t = b$. Thus,

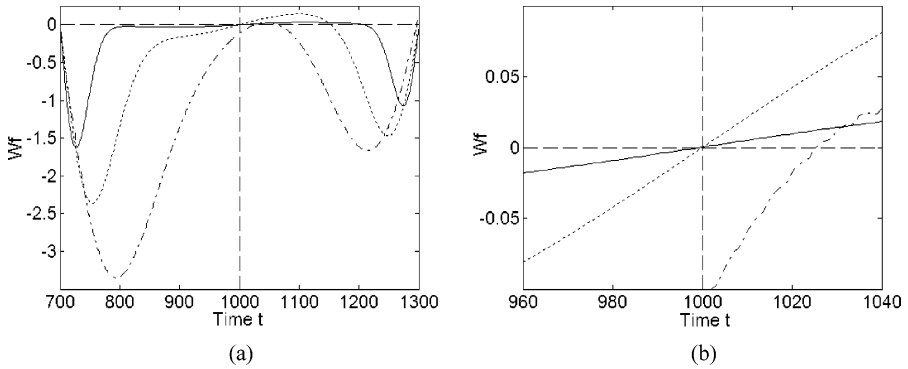

Figure 4. (a) WT at scales 37.5 (a_{min}, solid line), 75 (a_{max}, dotted line), and 128 (dash−dotted line). (b) Expanded view of the zero-crossing around $t = 1000$.

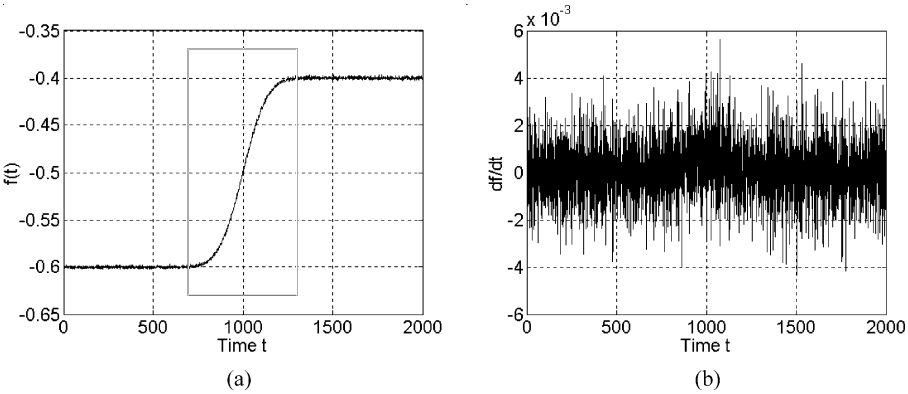

Figure 5. (a) Simulated sigmoidal signal with an added white Gaussian noise of standard deviation 0.001. (b) First derivative of the noisy signal.

for the sake of clarity in the discussion, the translation axis in the *Wf* graph was labeled as "Time *t*". The peaks on the left and right-hand side of the plot are caused by border effects. The peak on the left is larger because at this border the discontinuity of the signal with respect to zero is larger, as can be seen in Figure 2a (notice that the signal is negative). For convenience of visualization, a top view of the tridimensional WT plot is also shown in Figure 3b.

As can be seen, in the middle of the plots there is a valley, which is formed by zero crossings of WT and indicates the presence of an inflection point. A better characterization of the inflection point can be obtained by plotting cross sections of Figure 3a, as presented in Figure 4a for scales 37.5 (a_{min}), 75 (a_{max}), and 128. This figure shows that for each scale there are zero crossings with rising and falling behaviors. The zero crossing associated with the inflection point must have a rising behavior, because it is associated with the second derivative of the signal with a change in sign ($k = -1$ in eq 11). Thus, it can be concluded that the zero crossing with falling behavior is actually caused by a border effect and only the zero crossing around $t = 1000$ should be considered.

As can be seen from Figure 4b, the zero crossing occurs at exactly $t = 1000$ for scales a_{min} and a_{max}, which is in agreement with the discussion presented in the Theoretical Basis. Moreover, for $a = 128$, there is a shift to the right because the wavelet is so wide that its tail reaches the border at the right-hand side of the signal. That is the reason why scales larger than a_{max} should not be included in the analysis.

Detection in the Presence of Noise. To illustrate the robustness of the proposed wavelet detection technique, the effect of noise will be now investigated. Figure 5a presents a noisy signal, which was obtained by adding white Gaussian noise of zero mean and a standard deviation of 0.001 to the signal in Figure 2a. As can be seen in Figure 5b, the inflection point can no longer be localized from the first derivative plot.

The WT of this signal for scales a_{min} (37.5) and a_{max} (75) is depicted in Figure 6a, and an expanded view of the central zero-crossing region is presented in Figure 6b. As can be seen, the zero crossing still occurs at exactly $t = 1000$ even in the presence of noise.

Effect of Asymmetry around the Inflection Point. Figure 7 presents a simulated sigmoidal signal, which has an inflection point at $t = 1000$, as in the previous cases. The signal is asymmetric in that its slope varies differently before and after the inflection point. White Gaussian noise with zero mean and a standard deviation of 0.001 was added to the signal as in the preceding example.

Figure 8a depicts the WT of the asymmetric signal in the zero-crossing region of interest for the five scales considered in the analysis (a_{max}, $7a_{max}/8$, $6a_{max}/8$, $5a_{max}/8$, a_{min} as discussed in the Theoretical Basis section). As can be seen, unlike the previous examples, the position of the inflection point cannot be determined from the zero crossing of the WT for a single scale. However, the combined information of the different scales can be used in the proposed linear extrapolation procedure, as shown in Figure 8b. As can be seen, the extrapolation leads to 1004 as an estimate of the position of the inflection point.

To assess the sensitivity of the estimate provided by the proposed strategy with respect to noise, 1000 simulations

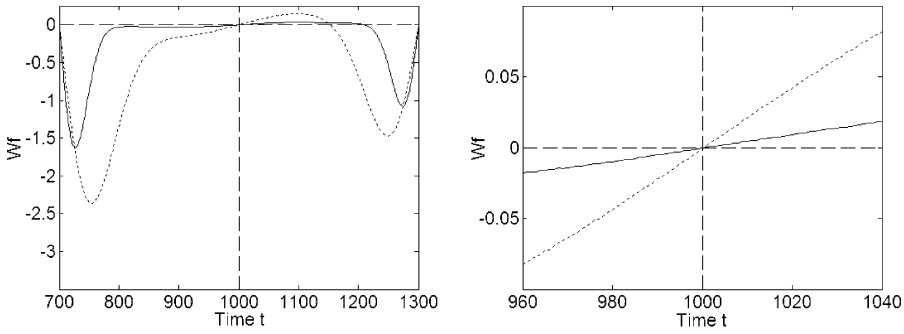

Figure 6. (a) WT of the noisy signal at scales 37.5 (a_{min}, solid line) and 75 (a_{max}, dotted line). (b) Expanded view of the zero-crossing around $t = 1000$.

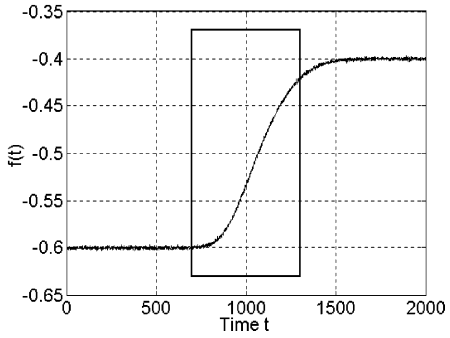

Figure 7. Simulated asymmetric sigmoidal signal with an added white Gaussian noise of standard deviation 0.001.

were carried out in a Monte Carlo fashion by adding different noise realizations to the asymmetric sigmoidal curve considered in this example. The results are presented in Figure 9 in the form of a histogram. As can be seen, the estimates of the position of the inflection point are located around the expected value. In fact, the average result of the 1000 simulations was exactly $t = 1000$ with a standard deviation of 10. This finding shows that the estimate yielded by the proposed strategy is unbiased.

Finally, it is interesting to place some remarks regarding the effective support width of the mother wavelet. Figure 8a shows that, as the scale gets smaller, the slope of the WT around the zero-crossing decreases and the zero-crossing position becomes less reliable, as mentioned in the Theoretical Basis. In the proposed procedure, the smallest scale for the analysis is determined as $a_{min} = d/(4S)$, where S is the effective support width adopted for the mother wavelet. In the examples presented above, S was taken as 4 and thus $a_{min} = d/16$. If a larger S was adopted, the analysis would move to smaller scales, and the effect of noise would be more pronounced. For instance, by setting $S = 6$ (instead of 4) and repeating the Monte Carlo simulation as above, the average result of the 1000 simulations is $t = 999$ with a standard deviation of 20 (instead of 10).

On the other hand, if a smaller S was adopted, one might risk having border effect interferences in the determination of the inflection point because a substantial part of the wavelet tail would fall outside the time interval in which the analysis is performed. The value $S = 4$ for the Mexican Hat wavelet was found to be a reasonable choice and led to good results in the PSA application considered in this work.

EXPERIMENTAL SECTION

Apparatus. A lab-made potentiostat/galvanostat connected to a Metrohm model 663 VA Stand for polarographic and voltametric analysis and to a personal computer was used for PSA measurements. All operations and experimental parameters were controlled by the software of the potentiostat/galvanostat.

The electrochemical cell consisted of a glass vessel in which three electrodes were inserted. A rotating glassy carbon electrode, a platinum rod, and an Ag/AgCl 3 mol L^{-1} KCl electrode were used as the working, counter, and reference electrode, respectively. All experiments were performed at room temperature (25 ± 1 °C).

Reagents, Samples, and Solutions. Deionized water purified with a Milli-Q Plus system (Millipore) and high purity reagents were used. The 2000 mg L^{-1} Hg(II) stock solution was prepared from mercury(II) chloride salt (Merck, Germany) in 0.1 mol L^{-1} HCl. The 1000 mg L^{-1} Cd(II) and Pb(II) stock solutions were prepared from their Titrisol (Merck, Germany) ampules in 0.1 mol L^{-1} HCl. The working standard addition solution, containing Pb(II) and Cd(II) with equal concentrations (10.0 mg L^{-1}), was prepared by diluting stock solutions in 0.1 mol L^{-1} HCl. In the same way, two synthetic samples, containing the analytes with equal concentrations of 25 and 50 μg L^{-1} were prepared in 0.1 mol L^{-1} HCl and 50 mg L^{-1} Hg(II).

Working Electrode Pretreatment. Before mercury film deposition (plating), the glassy carbon electrode was polished with alumina 3 μm, cleaned with 95% ethanol, and finally rinsed with deionized water.

Analytical procedure. About 10 mL of the nondeaerated synthetic sample was added into the measuring vessel, and the mercury film deposition was performed in stirred solution at −1.0 V for 5 min. The analyte deposition was initiated by applying a potential of −1.0 V at the working electrode during 30 s in a stirred solution. Subsequently, this potential was kept during 10 s without agitation, and then a stripping from −1.0 to −0.1 V was carried out. Immediately thereafter, a −0.1 V standby potential was applied to the electrolytic cell in order to maintain the integrity of the mercury film. The same process was repeated for three increasing levels of standard addition. The stripping measurements were always carried out in triplicate.

Between each sample analysis, the used film was mechanically removed, and the glassy carbon surface was polished with a wet filter paper before another plating.

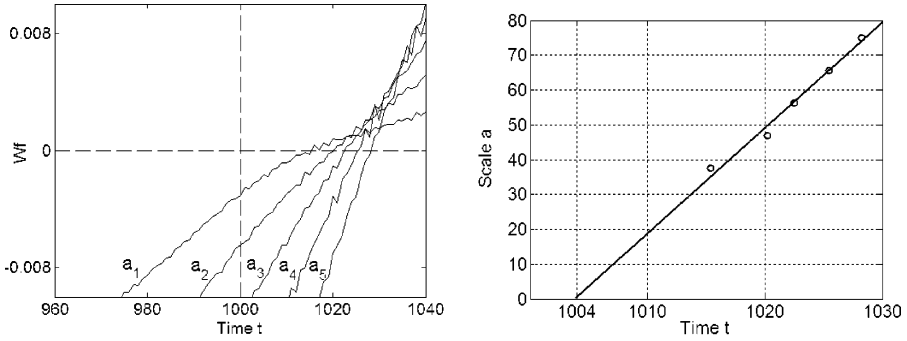

(a) (b)

Figure 8. (a) WT of the asymmetric noisy signal at fixed scale values ($a_1 = 37.5$, $a_2 = 46.875$, $a_3 = 56.25$, $a_4 = 65.625$, $a_5 = 75$). (b) Extrapolation graph adjusted to the zero crossing obtained at the five scales employed.

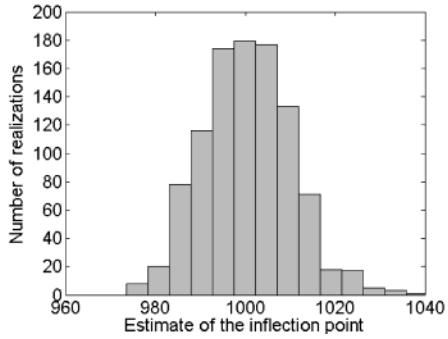

Figure 9. Histogram of the Monte Carlo simulation results (1000 realizations).

Software. Matlab 6.1 and its Wavelet Toolbox were used in all calculations.

RESULTS AND DISCUSSION

A potential-versus-time curve of a sample containing equal concentrations (50 μg l^{-1}) of Pb(II) and Cd(II) is presented in Figure 10a. The time interval between the stripping of the analytes, which is defined on the basis of the inflection points of the potential plateaus, is the analytical parameter that is proportional to the analyte concentration.[22,23] However, those inflection points can hardly be seen in the first derivative curve (Figure 10b), thus preventing an accurate measurement of the time interval between analyte stripping. Filtering techniques may be employed to minimize the noise, but in general they have the side effect of displacing the peaks. To overcome this problem, the proposed WT strategy was applied to the PSA curves. The gray boxes in Figure 10a,b indicate a region that will be used for illustration of the proposed procedure for inflection point localization.

Figure 11a shows an expanded view of the PSA curve region selected for analysis. In this case, the width of the analysis window is $d = 5174-4469 = 705$. Thus, the maximum and minimum scales to be employed are $a_{max} = d/8 = 88$ and $a_{min} = a_{max}/2 = 44$, respectively. Figure 11b shows the WT result at the five scales employed in the analysis (a_{max}, $7a_{max}/8$, $6a_{max}/8$, $5a_{max}/8$, a_{min}). As can be seen, there are zero-crossings with a rising behavior in the range 4800−5000 time counts, which are associated to the inflection point needed for PSA.

Figure 12a shows an expanded view of the zero-crossing region of interest. The zero-crossing positions were used to build a straight line that allows the localization of the inflection point, as shown in Figure 12b. As can be seen, in this case the extrapolation leads to an estimate of 4892 time counts as the position of the desired inflection point. It is worth noting that the extrapolation line has a negative slope in this case, unlike the line obtained in the simulated example (Figure 8b). This difference is due to the fact that the PSA curve in Figure 11a and the simulated curve in Figure 7 have different types of asymmetry. The PSA curve has a sharper concavity at its right-hand side, whereas the simulated curve exhibits the opposite behavior.

The results of applying the proposed WT-PSA strategy to two samples containing Cd(II) and Pb(II) in equal concentrations (25 and 50 μg L^{-1} in samples A and B, respectively) are presented in Table 1. For comparison, the values obtained by using the derivative PSA curve (DPSA) after a filtering procedure are also shown. In this case, several filtering techniques (Savitsky-Golay, Moving Average, Fourier Transform)[17] were tested, and the best results were obtained by using a Windowed Fourier Transform (WFT) with a 50-point window. The smoothing is accomplished by removing Fourier components with frequencies higher than $1/(50\Delta t)$ where Δt is the sampling time (5000 points s^{-1}). The frequency-domain apodization function was a parabola with a maximum of 1 at zero frequency and falling to zero at the cutoff frequency defined above.

The results in Table 1 show that WT-PSA and WFT-DPSA procedures led to similar results. In two cases (Pb in sample A and Cd and in sample B), WT-PSA resulted in more accurate determinations. Moreover, in the case of Pb in sample A, WT-PSA also resulted in a smaller standard deviation. In addition, it should be emphasized that the use of WT-PSA reduces the workload of the analyst, in comparison with traditional smoothing techniques, in that there is no need to choose appropriate filtering parameters (such as the technique to be employed as well as shape and width of the apodization function).

CONCLUSIONS

This paper proposed a novel multiscale strategy for localizing inflection points in signals, with emphasis on analytical applications. On the basis of a theoretical discussion and also of simulated examples, it was shown that the zero crossings of the WT of a signal can be used for the localization of the inflection point either directly (symmetric curves) or through a linear extrapolation procedure (asymmetric curves). The results of a Monte Carlo simulation for

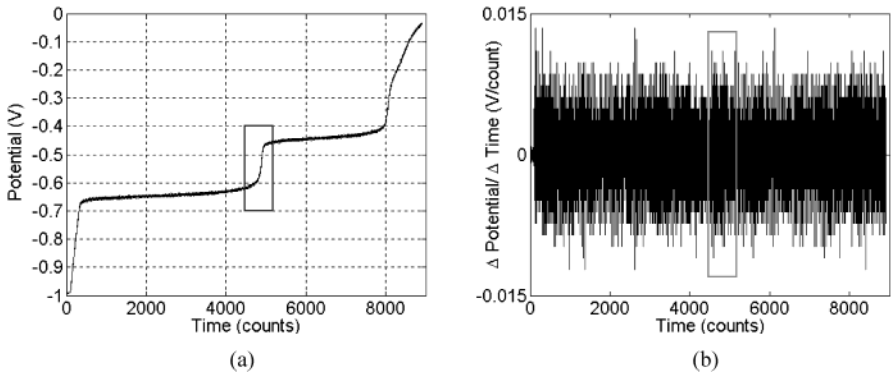

Figure 10. (a) Experimental PSA curve for a sample with equal concentrations (50 μg l^{-1}) of Pb and Cd. (b) First derivative of the PSA curve. The gray box in (a) and (b) indicates the region selected for analysis.

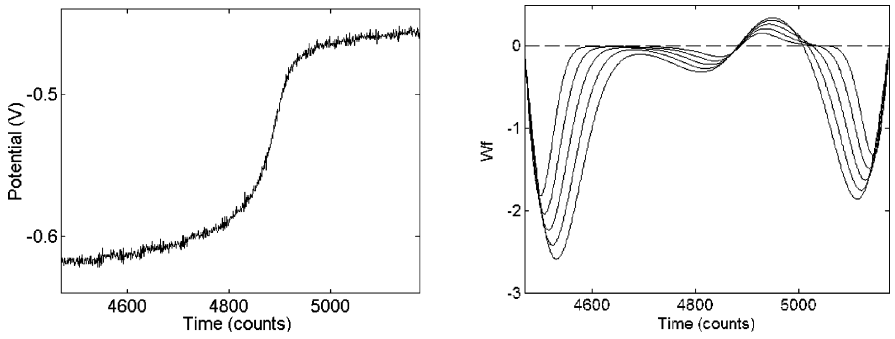

Figure 11. (a) Region selected for the analysis in the PSA curve. (b) WT of the selected region at the five scale values employed in the analysis (44, 55, 66, 77, 88).

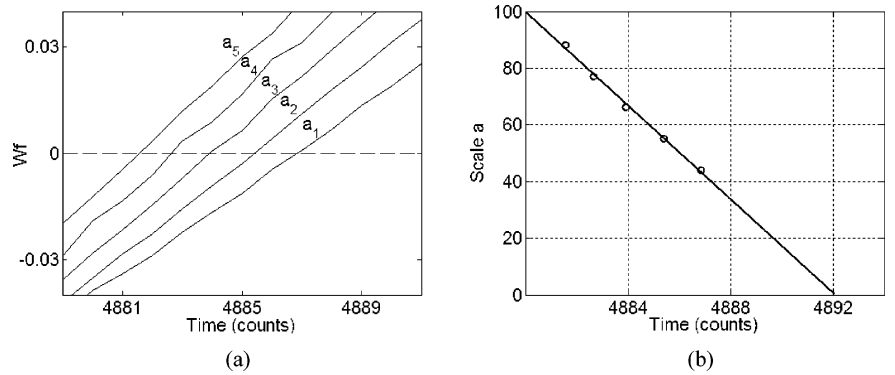

Figure 12. (a) Expanded view of the WT around the zero-crossing region of interest ($a_1 = 44$, $a_2 = 55$, $a_3 = 66$, $a_4 = 77$, $a_5 = 88$). (b) Extrapolation graph adjusted to the zero-crossing positions obtained at the five scales employed.

Table 1. Average Analyte Concentrations (μg L^{-1}) Obtained by the Proposed WT-PSA Strategy and by Analyzing the DPSA Curve after a WFT Smoothing[a]

	WT-PSA		WFT-DPSA		expected values	
sample	Cd	Pb	Cd	Pb	Cd	Pb
A	27 (±3)	25 (±1)	27 (±3)	26 (±3)	25	25
B	50 (±2)	48 (±1)	49 (±2)	48 (±1)	50	50

[a] The values in parentheses are standard deviations obtained from three repeated analyses.

noisy curves showed that the proposed strategy is unbiased in that its expected result is the actual position of the inflection point.

The utility of the proposed WT strategy was also demonstrated in a problem involving the determination of Pb and Cd with low concentration levels by PSA. In this application, it was found that the sigmoidal curves exhibited an asymmetric behavior, and thus the linear extrapolation process was needed. The WT-PSA results were in good agreement with the expected values and were slightly better than those obtained by analyzing the first derivative of the PSA curves after smoothing by a WFT. It is worth noting that the use of WT-PSA reduces the workload of the analyst, because it does not require a preliminary smoothing on the signal, which can be very time-consuming due to the need of an appropriate selection of the filtering parameters.

It is interesting to note that the asymmetric behavior verified in the PSA curves is also found in several analytical signals. For instance, potentiometric titration curves will only be symmetric if the participants in the titration react with one another in an equimolar ratio and also if the electrode reaction is perfectly reversible.[21] The former condition is lacking in many oxidation/reduction titrations, such as the

titration of iron(II) with permanganate.

Finally, it should be emphasized that, as demonstrated in the simulated examples, the proposed strategy works equally well for symmetric and asymmetric curves. Thus, it can be regarded as a general tool for the determination of inflection points.

ACKNOWLEDGMENT

The authors thank FINEP-CTPETRO (Proc. 0652/00) science funding program, PROCAD/CAPES (Proc. 0064/01-7), and PRONEX/CNPq (Proc. 015/98) for partial financial support. The research fellowships granted by the Brazilian agencies CNPq and CAPES are also gratefully acknowledged.

REFERENCES AND NOTES

(1) Brown, P. J.; Fearn, T.; Vannucci, M. Bayesian wavelet regression on curves with application to a spectroscopic calibration problem. *J. Am. Stat. Assoc*. **2001**, *96*, 398−408.
(2) Alsberg, B. K.; Woodward, A. M.; Winson, M. K.; Rowland, J. J.; Kell, D. B. Variable selection in wavelet regression models. *Anal. Chim. Acta* **1998**, *368*, 29−44.
(3) Depczynski, U.; Jetter, K.; Molt, K.; Niemoller, A. Quantitative analysis of near-infrared spectra by wavelet coefficient regression using a genetic algorithm. *Chemom. Intell. Lab. Syst*. **1999**, *47*, 179−187.
(4) Jetter, K.; Depczynski, U.; Molt, K.; Niemoller, A. Principles and applications of wavelet transformation of chemometrics. *Anal. Chim. Acta* **2000**, *420*, 169−180.
(5) Eriksson, L.; Trygg, J.; Johansson, E.; Bro, R.; Wold, S. Orthogonal signal correction, wavelet analysis, and multivariate calibration of complicated process fluorescence data. *Anal. Chim. Acta* **2000**, *420*, 181−195.
(6) Trygg, J.; Wold, S. PLS regression on wavelets compressed NIR spectra. *Chemom. Intell. Lab. Syst*. **1998**, *42*, 209−220.
(7) Vogt, F.; Tacke, M. Fast principal component analysis of large data sets. *Chemom. Intell. Lab. Syst*. **2001**, *59*, 1−18.
(8) Coelho, C. J.; Galvão, R. K. H.; Araújo, M. C. U.; Pimentel, M. F.; Silva, E. C. A linear semi-infinite programming strategy for constructing optimal wavelet transforms in multivariate calibration problems. *J. Chem. Inf. Comput. Sci*. **2003**, *43*, 928−933.
(9) Coelho, C. J.; Galvão, R. K. H.; Araújo, M. C. U.; Pimentel, M. F.; Silva, E. C. A Solution to the Wavelet Transform Optimization Problem in Multicomponent Analysis. *Chemom. Intell. Lab. Syst*. **2003**, *66*, 205−217.
(10) Mallat, S.; Hwang, W. L. Singularity detection and processing with wavelets. *IEEE Trans. Information Theory* **1992**, *38*, 617−643.
(11) Bakshi, B. R. Multiscale Analysis and Modeling Using Wavelets. *J. Chemom.* **1999**, *13*, 415−434.
(12) Liu, X. F.; Wang, H. G.; Huang, S. J.; Gu, H. C. Analysis of Electrochemical Noise with Wavelet Transform. *Corrosion* **2001**, *57*, 843−852.
(13) Liew, K. M.; Wang, Q. Application of Wavelet Theory for Crack Identification in Structures. *J. Eng. Mechan.* **1998**, *124*, 152−157.
(14) Li, C. W.; Zheng, C. X.; Tai, C. F. Detection of ECG characteristic points using wavelet transforms. *IEEE Trans. Biom. Eng.* **1995**, *42*, 21−28.
(15) Smrcok, L.; Durik, M.; Jorik, V. Wavelet Denoising of Powder Diffraction Patterns. *Powder Diffrac*. **1999**, *14*, 300−304.
(16) Galvão, R. K. H.; Araújo, M. C. U.; Saldanha, T. C. B.; Visani, V.; Pimentel, M. F. Estudo Comparativo sobre Filtragem de Sinais Instrumentais Usando Transformadas de Fourier e Wavelet. *Quim. Nova* **2001**, *24*, 874−884.
(17) Beebe, K. R.; Pell, R. J.; Seasholtz, M. B. *Chemometrics: A Practical Guide*; John Wiley: New York, 1998.
(18) Sadler, D. A.; Boulo, P. R.; Soraghan, J. S.; Littlejohn, D. Tutorial guide to the use of wavelet transforms to determine peak shape parameters for interference detection in graphite-furnace atomic absorption spectrometry. *Spectrochim. Acta B* **1998**, *53*, 821−835.
(19) Sadler, D. A.; Littlejohn, D.; Boulo, P. R.; Soraghan, J. S. Application of wavelet transforms to determine peak shape parameters for interference detection in graphite-furnace atomic absorption spectrometry. *Spectrochim. Acta B* **1998**, *53*, 1015−1030.
(20) Bos, M.; Hoogendam, E. Wavelet Transform for the Evaluation of Peak Intensities in Flow-Injection Analysis. *Anal. Chim. Acta* **1992**, *267*, 73−80.
(21) Skoog, D. A.; West, D. M.; Holler, F. J. *Fundamentals of Analytical Chemistry*; Saunders College Publishing: Fort Worth, 1992.
(22) Estela, J. M.; Tomás, C.; Cladera, A.; Cerdá, V. Potentiometric Stripping Analysis: A Review. *Crit. Rev. Anal. Chem.* **1995**, *25*, 91−141
(23) Jagner, D. Potentiometric Stripping Analysis − A Review. *Analyst* **1982**, *107*, 593−599.
(24) Daubechies, I. *Ten Lectures on Wavelets*; Society for Industrial and Applied Mathematics: Philadelphia, 1992.
(25) Alsberg, B. K.; Woodward, A. M.; Kell, D. B. An introduction to wavelet transforms for chemometricians: A time-frequency approach. *Chemom. Intell. Lab. Syst.* **1997**, *37*, 215−239.
(26) Rioul, O.; Vetterli, M. Wavelets and Signal Processing. *IEEE Signal Proc. Mag.* **1991**, *8*, 14−38.
(27) Walczak, B. *Wavelets in Chemistry*; Elsevier Science: New York, 2000.
(28) Carlson, B.; Carson, B.; Crilly, P. B.; Rutledge, J. C. *Communication Systems*; McGraw-Hill: New York, 2001.

CI034112W